Monthly Notices
of the
ROYAL ASTRONOMICAL SOCIETY

MNRAS **496,** 1343–1354 (2020)
Advance Access publication 2020 June 5

doi:10.1093/mnras/staa1569

Study of the effects of magnetic braking on the lithium abundances of the Sun and solar-type stars

R. Caballero Navarro [1]★ A. García Hernández [1,2]★ A. Ayala[2] and J. C. Suárez [1,2]

[1] *Department of Theoretical Physics and Cosmology, University of Granada (UGR), E-18071 Granada, Spain*
[2] *Instituto de Astrofísica de Andalucía (CSIC), Glorieta de la Astronomía S/N, E-18008 Granada, Spain*

Accepted 2020 May 29. Received 2020 April 17; in original form 2019 November 30

ABSTRACT

The study of lithium (Li) surface abundance in the Sun and young stellar globular clusters which are seemingly anomalous in present-day scenarios, as well as the influence of rotation and magnetic braking (MB) on its depletion during pre-main sequence (PMS) and main sequence (MS). In this work, the effects of rotational mixing and of the rotational hydrostatic effects on Li abundances are studied by simulating several grids of PMS and MS rotating and non-rotating models. Those effects are combined with the additional impact of the MB (with magnetic field intensities ranging between 3.0 and 5.0 G). The data obtained from simulations are confronted by comparing different stellar parameters. The results show that the surface Li abundance for the Sun-like models at the end of the PMS and throughout the MS decreases when rotational effects are included, that is the Li depletion rate for rotating models is higher than for non-rotating ones. This effect is attenuated when the MB produced by a magnetic field is present. This physical phenomena impacts also the star effective temperature ($T_{\rm eff}$) and its location in the HR diagram. The impact of MB in Li depletion is sensitive to the magnetic field intensity: the higher it is, the lower the Li destruction. A direct link between the magnetic fields and the convective zone (CZ) size is observed: stronger magnetic fields produce shallower CZ's. This result suggests that MB effect must be taken into consideration during PMS if we aim to reproduce Li abundances in young clusters.

Key words: Sun: abundances – Sun: magnetic fields – Sun: rotation.

1 INTRODUCTION

Despite decades of theoretical efforts, a coherent explanation for the lithium (Li) abundance discrepancies detected in star clusters cannot be found. In young and old clusters, these differences have been documented for stars in both pre-main-sequence (PMS) and main-sequence (MS) evolutionary stages. Additionally, these theoretical models are not able to explain the abundances detected in the late stages of the MS (Tschäpe & Rüdiger 2001).

Standard models, models that include convection only as a mixing process and do not consider other transport options like diffusion or angular momentum loss (AML), have been mainly involved in the elaboration of these predictions (Sestito & Randich 2005). Li is destroyed at a temperature $T_{\rm Li} \approx 2.5 \times 10^6$ K when an Li atom collides with a proton producing two He atoms. That takes place during proton–proton type II reactions (P-P II), and is therefore directly destroyed in stellar envelopes when the temperature at the base of the convection zone (BCZ) reaches $T_{\rm Li}$. The Sun in particular and the solar-type stars in general are characterized by having a CZ that covers much of the stellar radius during the PMS which causes that their lower limit to exceed $T_{\rm Li}$ (Iben 1965). This depletion stops during the approach to the zero-age MS (ZAMS) when the convection zone retreats and the temperature at BCZ is cooler than $T_{\rm Li}$. In the standard models only, the mass and the initial chemical composition determine at what distance from the stellar surface $T_{\rm Li}$ temperature is reached. Therefore stars with similar mass belonging clusters are expected to reach the ZAMS with equal surface Li abundances. Furthermore, they should also show a very similar Li evolution until their approach to the terminal-age MS (TAMS). During this period, the convection mechanisms unleash a mixing process that homogenizes the chemical composition of the envelope, from its lower limit till the star surface. However, different abundances of Li have been observed for different stellar populations (see Somers & Pinsonneault 2014, and references therein).

Theoretical models take initial Li abundance as an input parameter and only describe how it is exhausted. Therefore, in order to make an accurate estimate of the initial abundance of Li, it is a pre-requisite to be able to compare observations and models beforehand. Our Sun represents a unique exception, since it allows us to know the current abundance of this element in its photosphere, $A(^7\mathrm{Li}) = 1.1 \pm 0.1$ dex (Jeffries 2004), where $A(^7\mathrm{Li})$

★ E-mail: rcaballeron@correo.ugr.es (RCN); agh@ugr.es (AGH)

is defined

$$A(^7\mathrm{Li}) = \log(N_{^7\mathrm{Li}}/N_{^1\mathrm{H}}) + 12 \quad (1)$$

and its initial abundance of $A(^7\mathrm{Li}) = 3.34$ dex is obtained from meteorite measurements (Randich & Pasquini 2006). For other stars, the initial Li abundance is found to be in the interval 3.0 dex $< A(^7\mathrm{Li}) <$ 3.4 dex. This has been estimated from Randich & Pasquini (2006).

The impact of rotation both on PMS and Li depletion for solar-type stars has already extensively debated in the past (Pinsonneault 1997; Jeffries 2004; Somers & Pinsonneault 2014) and revised more recently on the basis of the availability of more accurate measures (Bouvier et al. 2016). However, these previous studies focused mainly on the hydrostatic effects and did not consider the influence of a coupling between the stellar magnetic field and its possible spin-down effect. AML has a direct influence in the mixing processes. It can be produced by a number of relevant mechanisms: mass loss, magnetic fields, and gravity waves (g modes). Gravity waves (Charbonnel & Talon 2005) and magnetic fields (Eggenberger, Maeder & Meynet 2009) transmit angular momentum (AM) much more effectively than inducing mixing (Denissenkov & Pinsonneault 2007). As a consequence, the amount of differential rotation between the radiative and the convective zones (CZs) of the star is reduced. Additionally, magnetic fields would also originate in the limits between these zones, in the so-called tachoclines (Aschwanden 2014; Guerrero et al. 2016), which interact with the solar wind particles that are forced to corotate with it. This slows down the star, effect which is known as magnetic braking (MB).

Today, standard models are not able to replicate the observed values of Li abundance on stellar surfaces. This might happen because certain physical mechanisms that influence the destruction of Li are either being modelled improperly or simply not being taken into account, for example, the MB. In this paper, we study the interactions between rotation and magnetic fields when it comes to discuss the AM distribution.

2 METHOD

In the remainder of this paper, we describe a semi-empirical approach for the calculation of the AML as a result of the torque applied by a magnetically coupled stellar winds. This has been implemented as an extension to Modules for Experiments in Stellar Astrophysics stellar evolution code (MESA; Paxton et al. 2010, 2013, 2015, 2018, 2019).

2.1 Modelling magnetic braking

We start by enumerating the most relevant aspects and assumptions made in modelling the evolution of rotation, MB, and AM in MESA. These will be considered for the calculation of the AML as a result of the torque applied by a magnetically coupled stellar winds.

A relevant parameter to characterize the influence of a given magnetic field on the stellar wind is the denominated wind confinement magnetic parameter (η_*). It represents a energy ratio (equation 2) and defines a characteristic parameter for the relative effectiveness of the magnetic fields in circumscribing and/or channelling the wind outflow (Ud-Doula & Owocki 2002).

$$\eta_* = \frac{B^2/8\pi}{\rho v^2/2} \quad (2)$$

where $B^2/8\pi$ is the magnetic field energy density, $\frac{1}{2}\rho v^2$ the kinetic energy density, B the magnetic field intensity, ρ the mass density, and v the stellar wind velocity.

Stars with similar initial masses but different mass loss ($\dot{M}$) ratios will end up evolving very differently. The ionized particles carried by the solar wind not only contribute to the mass loss but also to the loss of kinetic (K_e) energy that is deposited in the interstellar medium (ISM). Given a star with a spherically symmetric wind, $\dot{M}$ is characterized by the following expression:

$$\dot{M} = 4\pi r^2 \rho v \quad (3)$$

Using equations (2) and (3), η_* can be approximated by:

$$\eta_* = \frac{B^2 r^2}{\dot{M} v} \quad (4)$$

In general, a magnetically channeled outflow has a complex stream geometry but for convenience, the equation (3) simply characterizes the wind strength in terms of a spherically symmetric mass-loss rate. v can be characterized by the radial variation of outflow velocity in terms of the velocity law (equation 5)

$$v(r) = v_\infty(1 - R_*/r) \quad (5)$$

where r represents the distance from the centre of the star to the point where the velocity is to be measured, R_* is the radius of the star, and v_∞ is the terminal wind velocity. v_∞ is defined as the velocity that the wind reaches at large distance from the central star, where it is not accelerated anymore by the wind driving force but its deceleration due to interaction with the ISM is negligible (Niedzielski & Skórzynski 2002).

The line-driven winds of OB stars have terminal velocities that scale with the photospheric escape velocity (Lamers & Cassinelli 2000) according to:

$$v_\infty \simeq 1.92\ v_{\mathrm{esc}} \quad (6)$$

$$v_{\mathrm{esc}} = \sqrt{\frac{2\,G\,M_*}{R_*}} \quad (7)$$

where equation (7) describes the Newtonian escape velocity from the stellar surface, where G is the gravitational constant, R_* the radius, and M_* the mass of the star.

Making use of equation (7), v_∞ can be reformulated as:

$$v_\infty \simeq 1.92 \times 618 \left(\sqrt{\frac{R_\odot}{R_*}\frac{M_*}{M_\odot}}\right) \quad (8)$$

where $R_\odot$ is the radius, and $M_\odot$ the mass of the Sun.

It has been observed that strongly magnetic intermediate-mass stars typically have rotation rates much slower than other stars in their parent population (Mathys & Gautier 2006). In those stars, the magnetic fields interacts with the mass loss, where the Alfvén radius (R_A) plays an important role. Making use of η_* (equation 2), R_A is defined as the point in which the magnetic field energy density and the kinetic energy density are balanced. In case that R_A is greater than the stellar radius, then the wind flow will have to follow the magnetic field. As a consequence, the material leaves the stellar surface with a higher specific AM, as the corotation radius has increased and it roughly corresponds to R_A. Following Weber & Davis (1967), the AML can be calculated by:

$$\dot{J} = \frac{2}{3}\dot{M}\Omega R_A^2 \quad (9)$$

where $\dot{M}$ is the mass-loss rate, Ω the angular velocity at star surface, and R_A the Alfvén radius.

Table 1. Summary of adopted physics in MESA (based on Choi et al. 2016).

Parameter	Adopted prescriptions and values
Solar abundance	$X_\odot = 0.7154$, $Y_\odot = 0.2703$, $Z_\odot = 0.0142$
Equation of state	OPAL+SCVH+MacDonald+HELM+PC
Opacity	OPAL Type I for $\log T \geq 4$
	Ferguson for $\log T \leq 4$
Reaction rates	JINA REACLIB
Boundary conditions	ATLAS12; τ=100 tables + photosphere
Diffusion	Track ^{1}H, ^{2}He, ^{7}Li, ^{7}Be
Rotation	Differential rotation at PMS and MS
Convection	MLT + Ledoux, $\alpha_{\rm MLT} = 1.82$
Overshoot	Time-dependent, diffusive,
	$f_{\rm ov,\,core} = 0.0160$,
	$f_{\rm ov,\,sh} = 0.0174$
Semiconvection	$\alpha_{\rm sc} = 0.1$
Thermohaline	$\alpha_{\rm th} = 666$
Rotational mixing	Include SH, ES, GSF, SSI, and DSI
Magnetic effects	MB based on idealized
	Monopole field
Magnetic field	B(G) variable between [3.0–5.0]
Mass loss	Activated, $\dot{M}_{\rm max} = 10^{-3}$ M$_\odot$ yr^{-1}
Angular moment loss	Activated, $\dot{J} = \frac{2}{3}\dot{M}\Omega R_A^2$

The above expression can be rewritten according to Ud-Doula, Owocki & Townsend (2008) so that it depends on the η_* instead of the R_A as follows:

$$\dot{J} = \frac{2}{3}\dot{M}\Omega R_*^2 \eta_* \tag{10}$$

which is a more convenient expression to be implemented in MESA because is based on values directly exposed during the simulations.

3 RESULTS

3.1 Mesh models

According to the formulation in the previous sections, the only two free parameters of our implementation are B and Ω. The numerical simulations traced the rotational history and $A(^7\mathrm{Li})$ of a 1 M$_\odot$ star for a variety of initial values for B and Ω (see also Table 1). MESA uses the shellular approach (Meynet & Maeder 1997) to account for hydrostatic effects of rotation into 1D stellar models.

We adopted solar-scaled abundances and assume Asplund et al. (2009) solar initial abundance ($Z = Z_{\odot,\,\rm pr\,=\,0.0142}$). We also adopted the following nominal values to express stellar properties values in SI units, $R_\odot = 6.957 \times 10^{10}$ cm and $M_\odot = 1.988 \times 10^{33}$ g which are consistent with IAU resolutions (Mamajek et al. 2015). For a detailed description of the physics adopted in this paper, we refer the reader to Choi et al. (2016). That work was used as starting point for ours regarding the parametrization of the MESA project which was calibrated to reproduce the measured element abundances on the solar surface.

The models included rotation during the PMS as there are evidences that advocate for a strong established relationship between Li destruction and rotation on that phase (Bouvier et al. 2016, 2018). We modelled rotation such as AML is computed as a result of the torque applied to the convection zone by a magnetically coupled wind. Additionally, we did not take into account either the influence of internal magnetic fields or their existence during the T-Tauri phase. We adopted a simple and pragmatic theoretical approach to establish when the star is reaching the ZAMS phase. The selected criterion was based on the simultaneous existence of an extensive convective layer and a radiative core. From this moment on, the MB routine was activated, acting as an additional mechanism to those existing in the MESA evolutionary code that participated in the star AML. We assumed that the magnetic field did not vary its intensity throughout the evolution of the star until it reached the TAMS. In addition, other rotation effects were also considered during the evolution of the models: the AM transport from the radiative interior to the convective envelope and the AM redistribution associated with changes in the internal structure during the process of contraction to the MS.

In this study, we focused on the indirect role played by the MB on the Li destruction. This is a consequence of its influence on the rotational history of solar-type stars. Our major objective was to check how MB could contribute to explain the evolution of Li in the Sun and other solar-type stars. A set of different scenarios with magnetic field strengths ranging between 3.0 and 5.0 G were exercised. We computed the evolution of 1 M$_\odot$ stellar models at solar initial metallicity with $\Omega/\Omega_{\rm crit}$ varying between 0.0084 and 0.0336. More advanced models for more complex arrangements of the magnetic field as well as the evolution of its intensity throughout the life of the star were left for later work.

As expressed by equation (10), the amount of AML depends on R_A (or alternatively on η_*), Ω, and $\dot{M}$. For large η_* value, the star undergoes a significant deceleration. We controlled the value of η_* in the models by varying the magnetic field (B) and the stellar rotation speed (Ω). With regards to $\dot{M}$ and as reported in Table 1, the empirical formula developed by Reimers (1975) for stars in the asymptotic giant branch (AGB) was used for calculating the mass loss. For a solar-type star, the $\dot{M}$ during MS is relatively small, about 10^{-14} M$_\odot$ yr^{-1} (Noerdlinger 2008).

MESA assigns an Ω value for each cell k (Ω_k) which is adjusted so that the resulting AM is retained after calculating the new mass of the cell k (m_k) and its distance to the centre of the star (r_k). After that, an AM value is assigned to each cell k (J_k). At this point, our MB turns on, modifying J_k. This was done by providing an additional contribution ($\dot{J}_k$). This contribution is the result of the external torque exerted by the magnetic field once it has been distributed among the different layers that make up the CZ as dictated by equation (11):

$$\dot{J}_k = \dot{J}_* \frac{m_k r_k^2}{m_* r_*^2} \tag{11}$$

3.2 Li evolution without MB

Fig. 1 shows the temporal evolution of surface Li abundance for several 1 M$_\odot$ models initialized with different rotational velocities. The simulations took into account the effects of rotation and AML caused by stellar winds but not those of MB. The purple star and square are the surface Li abundances for the present-day Sun (Asplund et al. 2009) and for the Pleiades, respectively (Sestito & Randich 2005).

Notice how the Li abundance in the star surface decreased over time for all simulated models. The solid black line represents the reference model that adopts the solar-calibrated envelope overshooting parameters as documented in Choi et al. (2016). All models burned too much Li before the ZAMS and therefore did not match with the Pleiades average surface Li abundance. Also remarkable was the fact that there were barely any differences between the different models in terms of the abundance of Li for much of the PMS. Only after one million years was Li destroyed to an accentuated degree, since the necessary temperature was not reached at BCZ before.

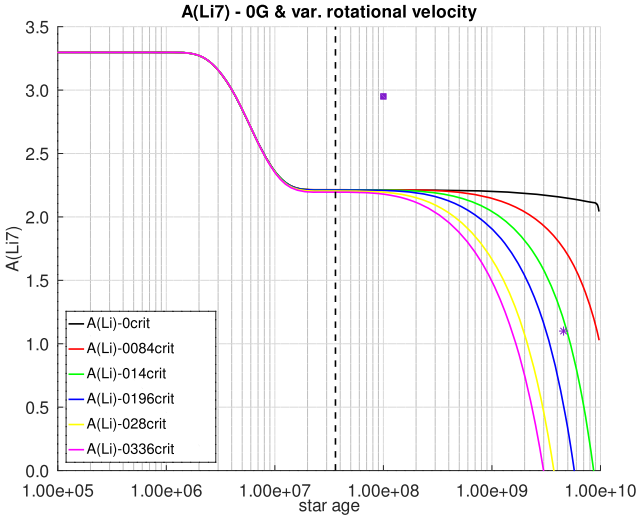

Figure 1. The evolution of surface ^{7}Li abundance relative to ^{1}H, as a function of time for several 1 $M_{\odot}$ models. The solid black line represents the reference model according to Choi et al. (2016). The rest of lines are models which include PMS rotation with Ω/Ω_{crit} between 0.0084 and 0.0336, respectively. The purple star and square are surface Li abundances for the present-day Sun (Asplund et al. 2009) and the average for the Pleiades cluster (Sestito & Randich 2005) respectively. The dashed vertical line makes reference to the ZAMS.

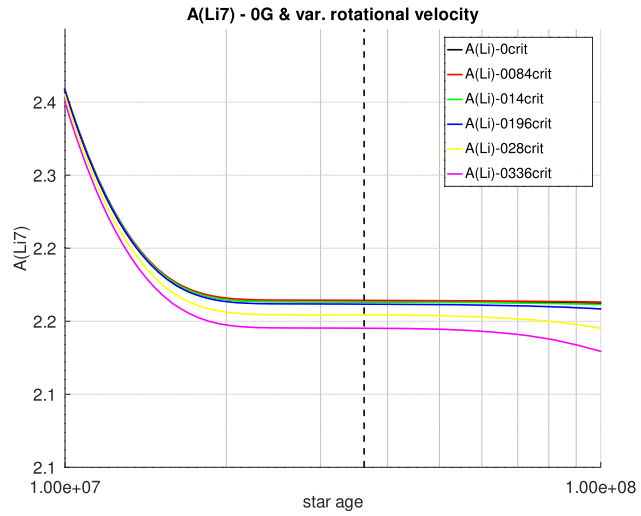

Figure 2. Similar to Fig. 1, but zooming-in on the ZAMS. The models with a higher initial rotational velocity reach already the ZAMS with a lower amount of Li measure on the star surface.

Afterwards, the different models destroyed the Li in a very similar way due to two main reasons. On the one hand, the CZs that the models developed had very similar sizes, so that the temperature at the BCZ was practically the same. On the other hand, the differential rotation between the core and the CZ did not begin to develop until it reached $\approx 10^{6}$ yr, achieving its maximum difference in the ZAMS about $\approx 10^{7}$ yr. It was at this moment that the combined effects of turbulence and rotational difference should increase, leading to notable differences in the evolution of A(Li) (see Fig. 2). Later, the reference model (black line) did not deplete Li efficiently on the MS

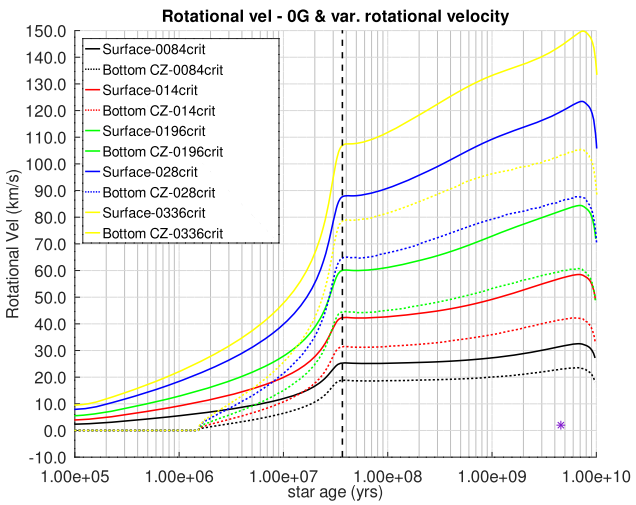

Figure 3. The evolution of angular velocity at surface (solid line) and at the bottom (dotted line) limit of the uppermost CZ, as a function of time for several 1 $M_{\odot}$ models. The models includes PMS rotation with Ω/Ω_{crit} values between 0.0084 and 0.0336. The purple star is the surface angular velocity for the present-day Sun (Gill 2012). The dashed vertical line makes reference to the ZAMS.

and failed (again) to match the current solar surface Li abundance. The other models which included rotation during the PMS with values of Ω/Ω_{crit} between 0.0084 and 0.0336 were able to burn Li in a more realistic way. Among them only one (green line) was close to match the present-day Li abundance of the Sun but its rotational velocity was much higher (see Fig. 3) than the 2 kms^{-1} of the Sun (Gill 2012).

For much of the PMS, the star rotated as a solid body (see Fig. 3) and this was because the star had a full convective interior. It was not until the end of the Hayashi track that the star began to develop a radiative core. It was in this stage when a difference in angular velocity appeared between the upper and lower limits of the radiative zone and CZ, respectively. The degree of differential rotation was directly influenced by the initial Ω. As the models were initialized with a higher angular velocity, the difference in velocity between the BCZ and the star surface was accentuated; the higher the initial velocity, the bigger the velocity gradient between the bottom and top limits of the CZ. As a consequence, the turbulence strength located at the BCZ increased so that Li could reach regions with temperatures about T_{Li} where it was finally burned and destroyed (see Fig. 1). Other investigations (Bouvier et al. 2018; Baraffe et al. 2017) point to a tendency diametrically opposed to the one exposed here, that is the faster the rotation speed, the greater the abundance of Li on the surface of the star.

Other well-known structural effects of rotation are the decrease of the effective temperature (T_{eff}) and to a less extent of stellar luminosity (L). Both effects can be observed graphically in the HR diagram of Fig. 4 which shows a zoomed-in view of evolutionary tracks from the ZAMS until the TAMS for several 1 $M_{\odot}$ models initialized with different rotational velocities. If we compare the non-rotating model (black solid line) with the rotating ones we can recognize that at the end of the PMS, the latter reach the ZAMS with a lower T_{eff} than the former. These results are in line with those of previous studies (see e.g. Pinsonneault et al. 1989; Piau & Turck-Chieze 2001; Eggenberger et al. 2012).

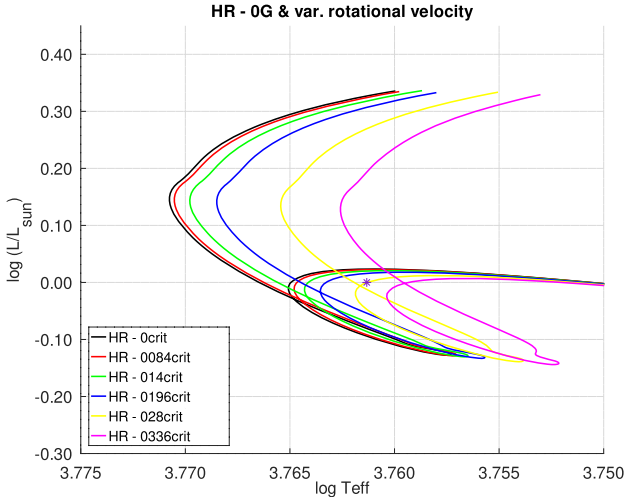

Figure 4. An example solar 1 $M_\odot$ grid of stellar evolutionary track from PMS till TAMS covering a wide range of angular velocities. The rotation is activated in the models in the PMS and those models reach before the ZAMS and at a lower $T_{\rm eff}$ than the non-rotating one (solid black line). The luminosity is expressed in terms of $L_\odot$.

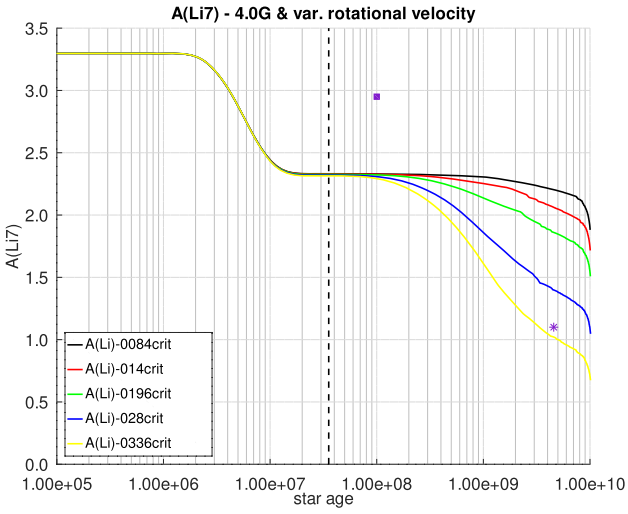

Figure 5. The evolution of surface ^{7}Li abundance relative to ^{1}H, as a function of time for several 1 $M_\odot$ models. The models include a magnetic field with an intensity of 4G and PMS rotation with $\Omega/\Omega_{\rm crit}$ between 0.0084 and 0.0336, respectively. The purple star and square are surface Li abundance for the present-day Sun (Asplund et al. 2009) and the Pleiades cluster (Sestito & Randich 2005), respectively. The dashed vertical line makes reference to the ZAMS.

3.3 Li evolution with MB

Fig. 5 shows the temporal evolution of surface Li abundance for several 1 $M_\odot$ models. Those models were initialized with different rotational velocities and took into consideration the effects of MB caused by a magnetic field of intensity 4G. If we compare it with Fig. 1 in which the effects of MB were neglected, we notice how the profiles of Li abundance were altered during PMS and MS. During the PMS, we can describe the effect as modest, somewhat expected and in line with the fact that the AML caused by MB (see equation 9) depends directly on the mass-loss rate. If we take into account that for solar-type stars, the models predict a modest total mass-loss rate, that value is even much lower in this phase. On the

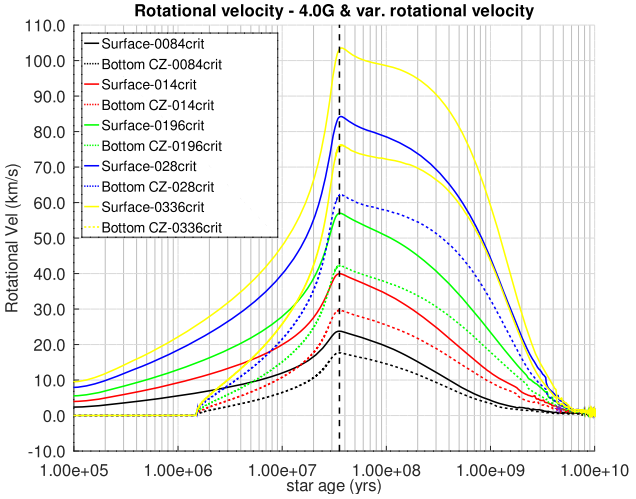

Figure 6. The evolution of surface rotational velocity, as a function of time for several 1 $M_\odot$ models. The models include a magnetic field with an intensity of 4 G, PMS rotation with $\Omega/\Omega_{\rm crit}$ between 0.0084 and 0.0336, respectively and MB. The purple star is the surface angular velocity for the present-day Sun (Gill 2012). The dashed vertical line makes reference to the ZAMS.

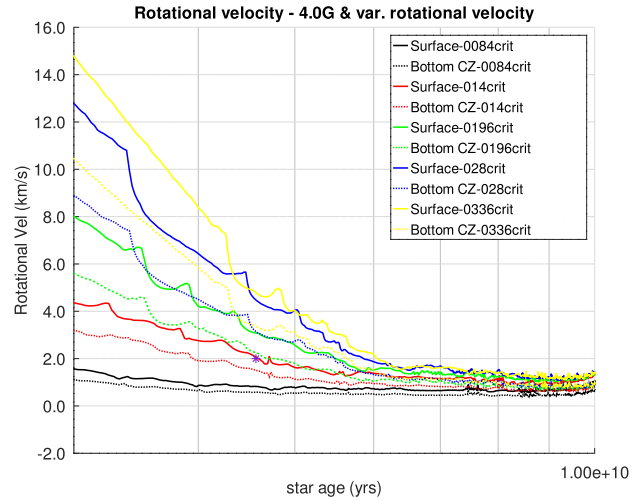

Figure 7. Similar to Fig. 6, but now showing in detail the surface rotational velocity as the star approaches TAMS.

contrary, during the MS it is observed that the AML is much more significant, causing a smaller amount of Li to be destroyed.

The effect of the MB routine can be seen even more clearly in Figs 6 and 7, and Appendices.[1] In those figures, we represented the rotation profiles for the surface of the stars and for the bottom of the convective envelope. They are 1 $M_\odot$ models initialized with different rotational velocities and considering the influence of MB. Similarly to the $A(^7{\rm Li})$ evolution profiles commented in the previous paragraph, the effect of the routine were visible once the ZAMS was reached. If we compare the evolution of the curves presented here

[1]The appendices comprise a series of grids as a function of time and for several 1 $M_\odot$ models in which on the one hand, the evolution of surface ^{7}Li abundance relative to ^{1}H for both variable magnetic field intensities and angular velocities and on the other hand, the evolution of surface rotational velocity are shown.

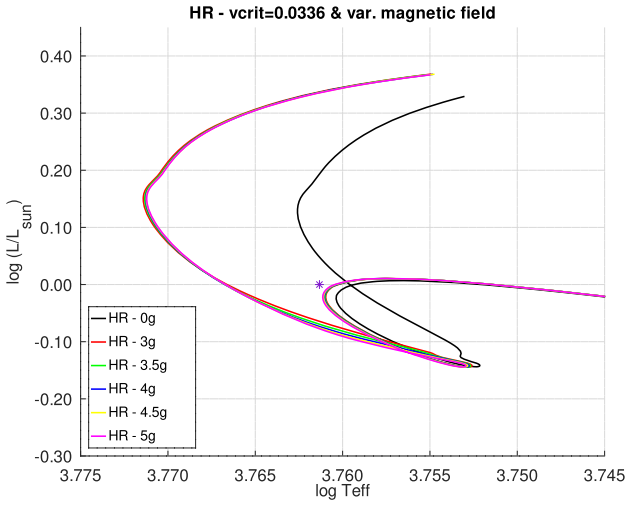

Figure 8. Similar to Fig. 4, but now showing in detail the effects of MB on the evolutionary tracks for different magnetic field strengths and $\Omega/\Omega_{\rm crit}$ = 0.0336. The presence of a magnetic field produces hotter stars due to the influence of the MB on the rotational velocity of the star.

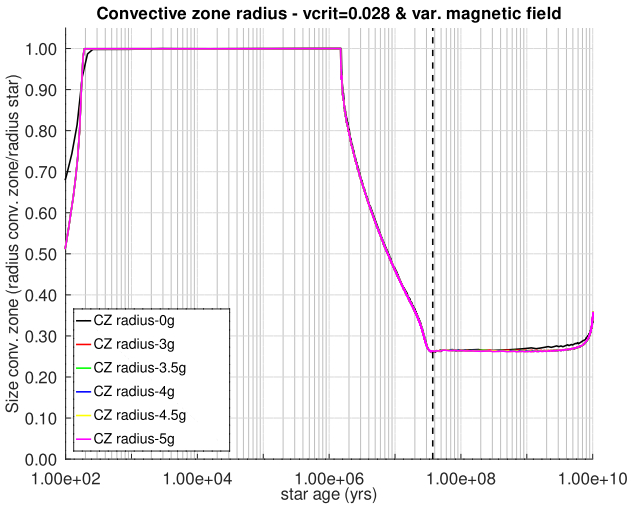

Figure 9. The evolution of CZ size as a function of time for several 1 $M_\odot$ models. The models were all initialized with $\Omega/\Omega_{\rm crit} = 0.0336$ and magnetic field strengths vary between 0.0 and 5.0 G. The dashed vertical line makes reference to the ZAMS.

with those of Fig. 3 we see how the star, instead of keep increasing Ω, began to slow down after having reached its maximum in the passage through the ZAMS. Notice that at this point, the angular velocities at the surface of the star and at the BCZ reached their maximum difference. On the other hand, the MB effect caused the angular velocities between both zones of the star to decrease until, for an age close to that of the Sun (see Fig. 7), the star practically rotated like a rigid solid. These results were also consistent with those obtained by Eggenberger, Maeder & Meynet (2010) as far as the effect of the magnetic field, in particular its influence on the loss of AM, has on the rotational velocity of the star.

In a similar way, we also observed that the models with lower angular velocity generally ended up exhibiting higher values for the Li abundance on the surface (see Fig. 5, and Figs A1 and A2). In none of those cases, we did obtain values of Li on the surface higher than those shown by the model without rotation.

The MB also left its mark on the HR diagram by significantly affecting the $T_{\rm eff}$ of the star. To visualize this effect, we take as reference Fig. 8 in which all models were started with the same value $\Omega/\Omega_{\rm crit} = 0.0336$, but the intensity of the simulated magnetic field was different. Notice that the models with MB produced hotter stars due to its influence. The lower speed with which the star rotated due to the MB effect caused the increase of the $T_{\rm eff}$, being this difference of practically 95 K between the simulated models with 0.0 and 5.0 G respectively for $\log(L/L_\odot) = 0$.

As described in Section 3.1, the MB routine distributed the total amount of AML calculated according to equation (11) among the different layers that composed the CZ. In Fig. 9, we can observe the evolution of the most external CZ normalized with respect to the radius of the star for several 1 $M_\odot$ models. The models were all initialized with $\Omega/\Omega_{\rm crit} = 0.0336$ and magnetic field strengths varying between 0.0 and 5.0 G. In accordance with the established models of stellar evolution, in a solar-type star the CZ covers practically all of it for a large part of the PMS. As it approaches the ZAMS, the CZ is decreasing as a consequence of the appearance of a radiative core and maintains an approximately constant radius until the final stage of the MS. In this point, it increases significantly as a response to the generalized expansion of the star's radius.

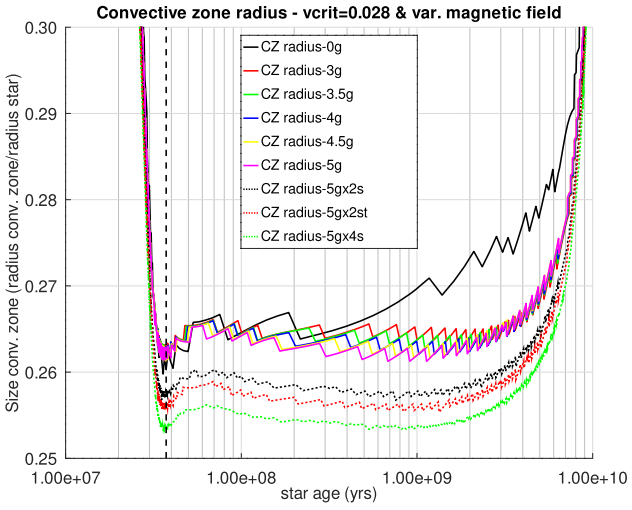

Figure 10. Similar to Fig. 9, but now showing in detail the size of the convection zone in the models from ZAMS up to TAMS. As the intensity of the magnetic field increases, the size of the CZ decreases. The first three pointed curves (below 0.26), have been artificially shifted downwards to illustrate the impact of the temporal (two times in time-step and number of shells, red dotted line) and spatial (two and four times number of shells, black and green dotted lines, respectively) resolution on the numerical solution for the 5 G case.

Regarding the effect of MB on the size of the CZ, we observe that as the intensity of the magnetic field increased, the size of the CZ decreased (see Fig. 10). The radiative core pushed outward to include a rapidly increasing fraction of the stellar mass, making that the temperature at the CZ base dropped below $T_{\rm Li}$. This effect was most evident during MS. The decrease in the size of the CZ was in line with the fact that less Li was destroyed by causing less stellar material to reach areas with temperatures above $T_{\rm Li}$.

Notice the jagged appearance in Fig. 10. We suspected a numerical origin for the wriggles. In order to check it out, we computed models for all the physical options considered with higher temporal (time-step) and spatial (number of shells) resolutions. For the sake

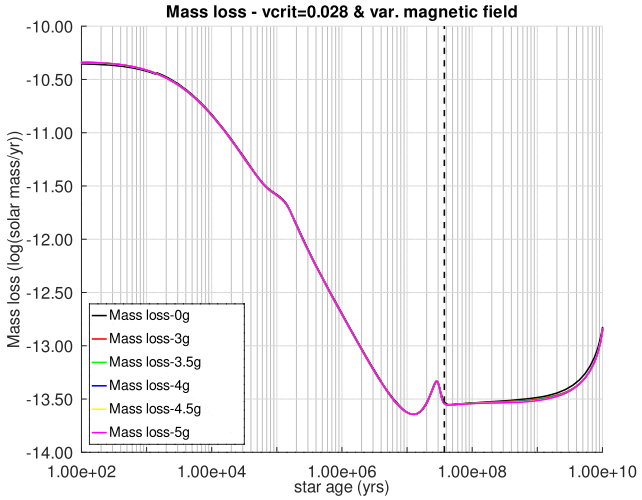

Figure 11. The evolution of mass loss $\dot{M}$ as a function of time for several 1 $M_\odot$ models. The models include different magnetic field intensity between 0.0 and 5.0 G and PMS rotation with $\Omega/\Omega_{\rm crit} = 0.028$. The dashed vertical line makes reference to the ZAMS.

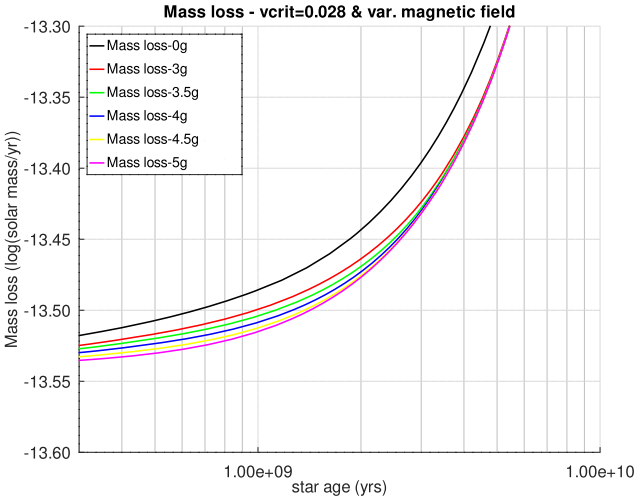

Figure 12. The evolution of mass loss $\dot{M}$ as the star is approaching TAMS, as a function of time for several 1 $M_\odot$ models. The models include a variable magnetic field intensity between 0.0 and 5.0 G and PMS rotation with $\Omega/\Omega_{\rm crit} = 0.028$. The stronger the magnetic field, the lower $\dot{M}$.

of visual clarity, we illustrated the impact on the numerical solutions only for the 5 G case, although the effects are the same in all cases. These are indicated as dotted lines in the figure, shifted-down just to become visible. Note that the larger the spatial resolution the smoother is the curve. The effect is less significant for the temporal resolution. The curve with two times in both spatial and temporal resolutions shows no difference with the case of two times in only the number of shells. The four times in spatial resolution points to the most appropriate number of shells to fine-track the evolution of the CZ. However such high resolution implies to significantly increase the computation time, with no effect in the final conclusions of this work. Indeed, the size of the zigzag features is around 10^{-3}, which is far below the convection time-scale and Li abundances measured in the stellar surface. It is thus save to neglect such effects by using the original time/space resolution.

In Fig. 11, we can see the evolution of $\dot{M}$ during PMS and MS for several 1 $M_\odot$ models. The models were all initialized with $\Omega/\Omega_{\rm crit} = 0.0336$ and magnetic field strengths varying between 0.0 and 5.0 G. In the first stages of PMS was where the greatest mass loss was concentrated and this diminished as it approached the ZAMS. Because the star also decreased its radius during the PMS, it increased Ω obeying the principle of conservation of AM. When reaching the ZAMS, the stellar radius remained more or less stable for much of the MS (except for its final stage, see Fig. 12) but continued to lose mass whilst increasing Ω, although in a less aggressive way if we compare it with the PMS. However, as a consequence of both the appearance of the radiative core during Henyey track and the existence of a CZ (see Fig. 13), the MB routine was activated, causing the angular velocity of the star to begin to decrease along the entire MS. The more intense the magnetic field, the greater the braking effect.

3.4 Alternative Li evolution with MB

Up to this point, the simulations of the different models were based on the parametrization gathered in Table 1, which in turn was adopted from Choi et al. (2016). If we recall the evolution of the Li shown in Figs 1 and 5, we highlighted that on both cases too much Li was burned before reaching the ZAMS and therefore did not

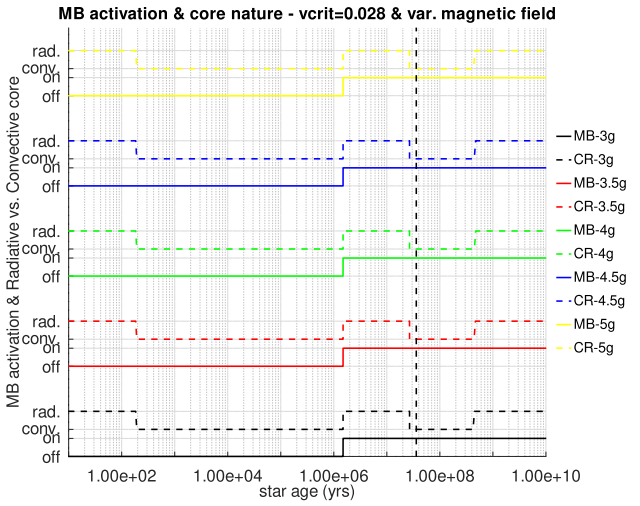

Figure 13. The activation of the MB routine as a function of the presence of a radiative core. The models include a magnetic field with an intensity ranging between 3.0 and 5.0 G and PMS rotation with $\Omega/\Omega_{\rm crit} = 0.0228$. The solid lines signal the MB routine activation (on) and deactivation (off). The horizontal dashed lines inform about the star's core nature: radiative (rad) or convective (conv). By implementation decision, once the routine is activated, it remains on even if the star's core nature change to convective. The dashed vertical line makes reference to the ZAMS.

Table 2. Alternative MTL and overshooting parameters.

Parameter	Adopted prescriptions and values
Convection	MLT + Ledoux, $\alpha_{\rm MLT} = 1.70$
Overshoot	Time-dependent, diffusive, $f_{\rm ov,\,core} = 0.016$, $f_{\rm ov,\,sh} = 0.002$

match with the Pleiades average surface Li abundance. On the other hand, using a parametrization slightly different from the one used until now in which the parameters of convection and overshooting have been readjusted according to Table 2, the simulations could

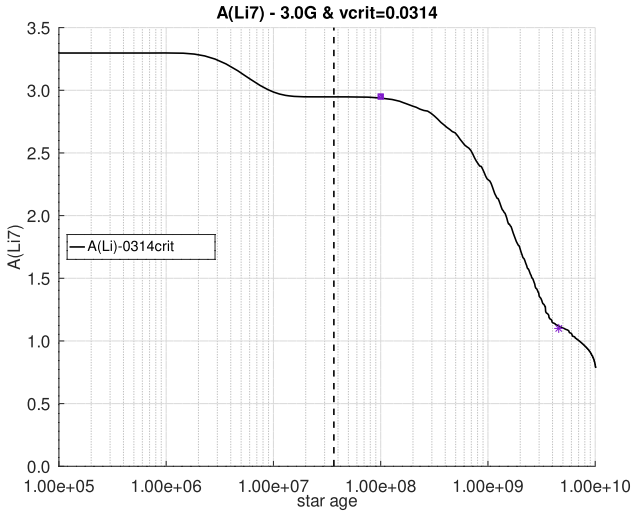

Figure 14. The evolution of surface ^{7}Li abundance relative to ^{1}H, as a function of time for a 1 $M_{\odot}$ model. The model include a magnetic field with an intensity of 3 G and PMS rotation with $\Omega/\Omega_{crit} = 0.0314$, respectively. MLT and overshooting parameters have been set to $\alpha_{MLT} = 1.70$, $f_{ov,\,core} = 0.016$, and $f_{ov,\,sh} = 0.002$. The purple star and square are surface Li abundance for the present-day Sun (Asplund et al. 2009) and the Pleiades cluster (Sestito & Randich 2005) respectively. The dashed vertical line makes reference to the ZAMS.

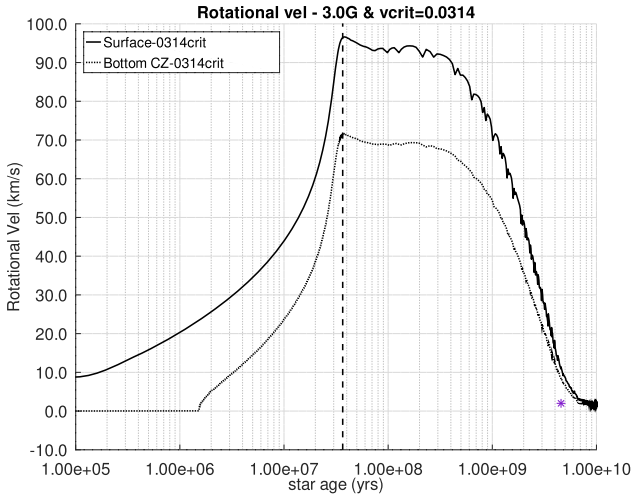

Figure 15. The evolution of surface rotational velocity, as a function of time for a 1 $M_{\odot}$ model. The model include a magnetic field with an intensity of 3 G, PMS rotation with $\Omega/\Omega_{crit} = 0.0314$, parameters in Table 2 and MB. The purple star is the surface angular velocity for the present-day Sun (Gill 2012). The dashed vertical line makes reference to the ZAMS.

reproduce more faithfully both the Pleiades cluster and the Sun Li abundances (see Fig. 14).

Similarly, the evolution of the angular velocity for this new configuration is shown in Fig. 15. Here we did not yet reproduce correctly the angular velocity of the Sun. It became evident that the influence of the free, relatively arbitrary, parameters associated with MLT significantly conditioned the evolution of the Li abundance. However, without the inclusion of MB, it was not possible to fit it for the Pleiades and the Sun with the same evolutionary track. This fact opens the door for other solar-compatible parametrizations to reproduce the observations in young stellar clusters and for the Sun.

4 CONCLUSIONS AND FUTURE WORKS

We have shown, through the different simulated stellar models, that the effects induced by the combination of both rotation and MB mechanisms offer a plausible way to reconcile the observational data with the theoretical models. The latter is of major importance both for the transport of AM and for the transport of chemical elements. We are also well aware that we are still far from understanding the exact physical mechanisms that govern these processes, so it is necessary to continue to delve into these areas of study. Particularly the study of the evolution of the magnetic fields during the PMS and MS and their impact on AML.

Future and improved implementations of our routine will be made to study the results on tracks, surface Li composition, rotation, etc. It is likely that in a rotating stellar model simulated with MB from the beginning, the differential rotation is very much reduced and therefore Li abundances observed in young stars could be properly explained. We propose that this result could be achieved by a law of interdependence between Ω and B. So that, during the PMS, when the star rotates faster, the MB effect is more efficient. On the other hand, during the MS, when the start slows down, the MB will become less intensive. This approach would establish a self-regulating mechanism over the angular velocity of the star that would end up directly influencing the Li evolution. It is equally important to understand better the general role of mass loss in AML and mostly in cooler, low-mass stars. Nowadays it is challenging to determine the terminal velocity of the stellar wind for this type of stars which plays a key role on the AML.

We emphasize as well that our models failed to match at the same time the observed solar Li abundance and Ω. We could not, therefore, ascertain to have correctly modelled the rotational history of the Sun. In view of these shortcomings in our models, we must analyse the results obtained with caution and not draw any premature conclusions. We have also shown how an alternative MLT parametrizations could produce results in line with the observations. The following conclusions have been supported in the course of this work:

(i) Inclusion of the magnetic field leads to cooler models and lower Li depletion in the MS.

(ii) A combination of rotation during the PMS and MB effect during MS produces different, potentially more promising behaviour than those produced by standard models. Thus, our approach points to reproduce the observed A(Li) and the solar rotational velocity at the same time.

(iii) T_{eff} from standard evolutionary tracks represent upper limits since these models do not take into consideration the MB effect nor rotation.

(iv) The CZ extension decreases when the intensity of the magnetic field increases.

(v) MB during PMS and/or adjustment of MLT overshooting and α_{MLT} free parameters seems to be also required for explaining Li abundances in young clusters.

The next steps will be focused on understanding how magnetic fields are linked to rotation, how their topologies are and how they evolve in time in order to go beyond the treatment on the MB routine that has been done in this work.

SOFTWARE

The simulations used in this paper been executed with the MESA release 10398.[2] The different figures have been generated making use of GNU Octave 5.1.0. [3]

ACKNOWLEDGEMENTS

We are pleased to acknowledge Jieun Choi her kindness in responding to the different questions about her work which were aimed to reproduce the results obtained as far as Li is concerned, and also for allowing us access to the MESA files she used. Also we very much appreciate the expert support provided by Elisa Delgado-Mena during the process review of this document. Similarly, we wish also to thank Matteo Cantiello and Bill Paxton for their very valuable support in the development of the MB routine in MESA. Finally, we wish to acknowledge the generous work and help offered by the MESA community. The authors acknowledge funding support from Spanish public funds (including FEDER funds) for research under projects ESP2017-87676-C5-2-R and ESP2017-87676-C5-5-R. JCS also acknowledges support from project RYC-2012-09913 under the 'Ramón y Cajal' program of the "Ministerio de Ciencia e Innovación".

REFERENCES

Aschwanden M. J., 2014, Encyclopedia of the Solar System, 3rd edn., p. 235
Asplund M., Grevesse N., Sauval A. J., Scott P., 2009, ARA&A, 47, 481
Baraffe I., Pratt J., Goffrey T., Constantino T., Folini D., Popov M. V., Walder R., Viallet M., 2017, ApJ, 845, L6
Bouvier J. et al., 2016, A&A, 590, 78
Bouvier J. et al., 2018, A&A, 613, 63
Charbonnel C., Talon S., 2005, Science, 309, 2189
Choi J., Dotter A., Conroy C., Cantiello M., Paxton B., Johnson B. D., 2016, AAS, 823, 106
Denissenkov P. A., Pinsonneault M., 2007, ApJ, 655, 1157
Eggenberger P., Maeder A., Meynet G., 2009, Proc. Int. Astron. Union, 5, 381
Eggenberger P., Maeder A., Meynet G., 2010, A&A, 519, L2
Eggenberger P., Haemmerlé L., Meynet G., Maeder A., 2012, A&A, 539, A79
Gill R. M., 2012, Technical Report, Rotation Period of the Sun-Gill The Rotational Period of the Sun Using the Doppler Shift of the Hydrogen alpha Spectral Line, Merritt Observatory, CA
Guerrero G. et al., 2016, ApJ, 819, 104
Iben I., 1965, ApJ, 141, 993
Jeffries R. D., 2004, Pre-Main-Sequence Lithium Depletion, Springer, Berlin Heidelberg
Lamers H. J. G. L. M., Cassinelli J. P., 2000, Introduction to Stellar Winds. Cambridge University Press, Cambridge
Mamajek E. E. et al., 2015, IAU Inter-Division A-GWorking Group on Nominal Units for Stellar & Planetary Astronomy
Mathys G., Gautier, 2006, Proc. Int. Astron. Union, 2, 285
Meynet G., Maeder A., 1997, A&A, 321, 465
Niedzielski A., Skórzynski W., 2002, Technical Report, Kinematical Structure of Wolf-Rayet Winds, Technical Report, N. Copernicus University, Poland
Noerdlinger P. D., 2008, St. Mary's University, Department of Astronomy and Physics Halifax, Canada
Paxton B. et al., 2013, ApJS, 208, 4
Paxton B. et al., 2015, ApJS, 220, 15
Paxton B. et al., 2018, ApJS, 234, 34
Paxton B. et al., 2019, ApJS, 243, 10
Paxton B., Bildsten L., Dotter A., Herwig F., Lesaffre P., Timmes F., 2010, ApJS, 192, 35
Piau L., Turck-Chieze S., 2001, ApJ, 566, 419
Pinsonneault M., 1997, ARA&A, 35, 557
Pinsonneault M. H., Kawaler S. D., Sofia S., Demarque P., 1989, ApJ, 338, 424
Randich S., Pasquini L., 2006, ESO Astrophys. Symp. Chemical Abundances and Mixing in Stars in the Milky Way and its Satellites. Springer, Berlin Heidelberg
Reimers D., 1975, in Probl. Stellar Atmos. Envel. Springer, Berlin Heidelberg, p. 229
Sestito P., Randich S., 2005, A&A, 442, 615
Somers G., Pinsonneault M., 2014, ApJ, 790, 72
Tschäpe R., Rüdiger G., 2001, A&A, 377, 84
Ud-Doula A., Owocki S. P., 2002, ApJ, 576, 413
Ud-Doula A., Owocki S. P., Townsend R. H. D., 2008, MNRAS, 392, 1022
Weber E. J., Davis L., 1967, The Angular Momentum of the Solar Wind, Technical Report, California Institute of Technology, Pasadena, CA

APPENDIX A: MESH MODELS VISUALIZATION

The following figures comprise a series of grids as a function of time and for several 1 $M_{\odot}$ models in which on the one hand, the evolution of surface ^{7}Li abundance relative to ^{1}H for both variable magnetic field intensities and angular velocities and on the other hand, the evolution of surface rotational velocity are shown.

[2] http://mesa.sourceforge.net/release/2018/03/21/r10398.html
[3] https://www.gnu.org/software/octave/

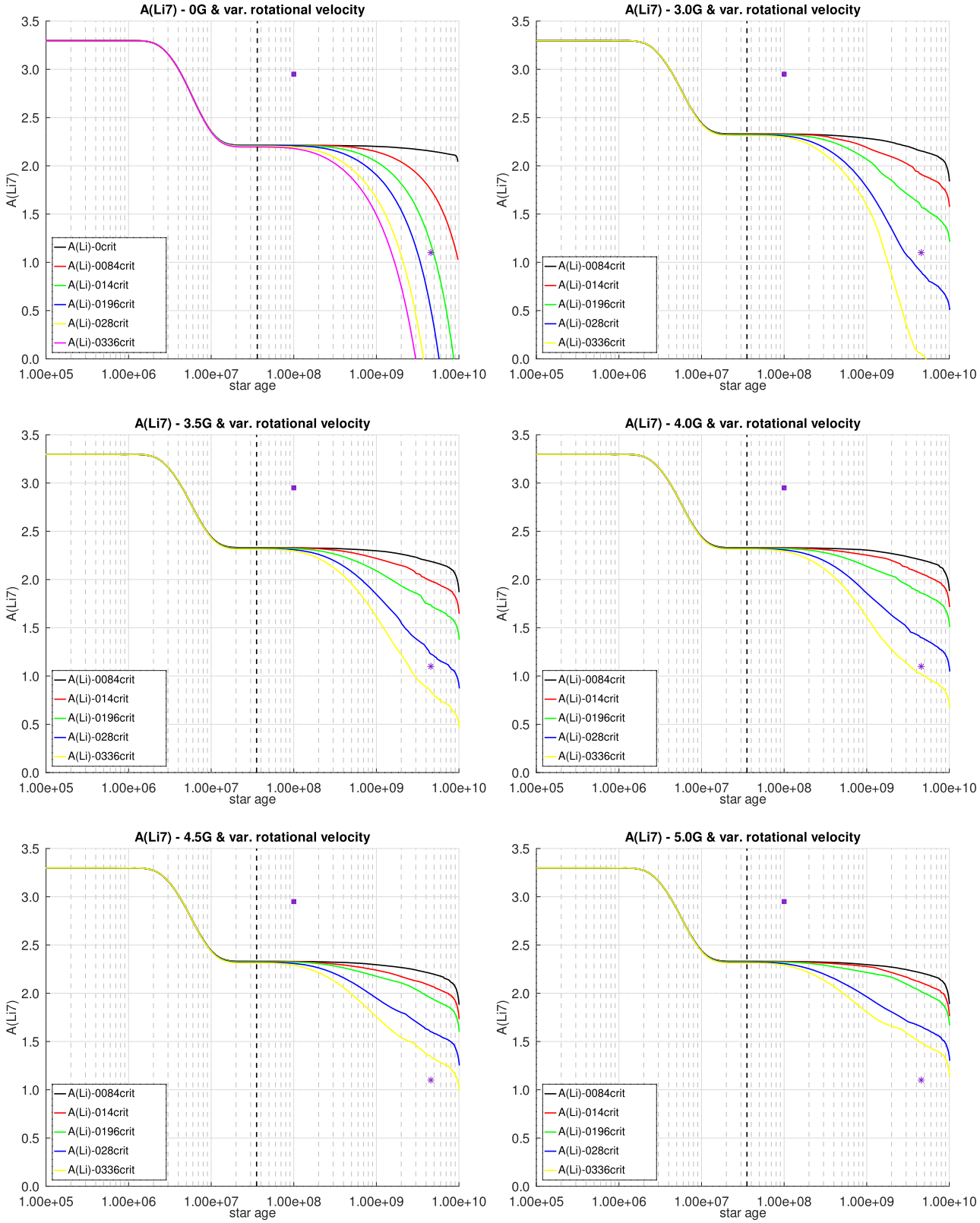

Figure A1. Grid showing the evolution of surface ^{7}Li abundance relative to ^{1}H, as a function of time for several 1 $M_{\odot}$ models. Each figure shows a set of models in which the magnetic field with intensity has been fixed and Ω/Ω_{crit} varies between 0.0084 and 0.0336, respectively. The purple star and square are surface Li abundance for the present-day Sun (Asplund et al. 2009) and the Pleiades cluster (Sestito & Randich 2005) respectively. The dashed vertical line makes reference to the ZAMS.

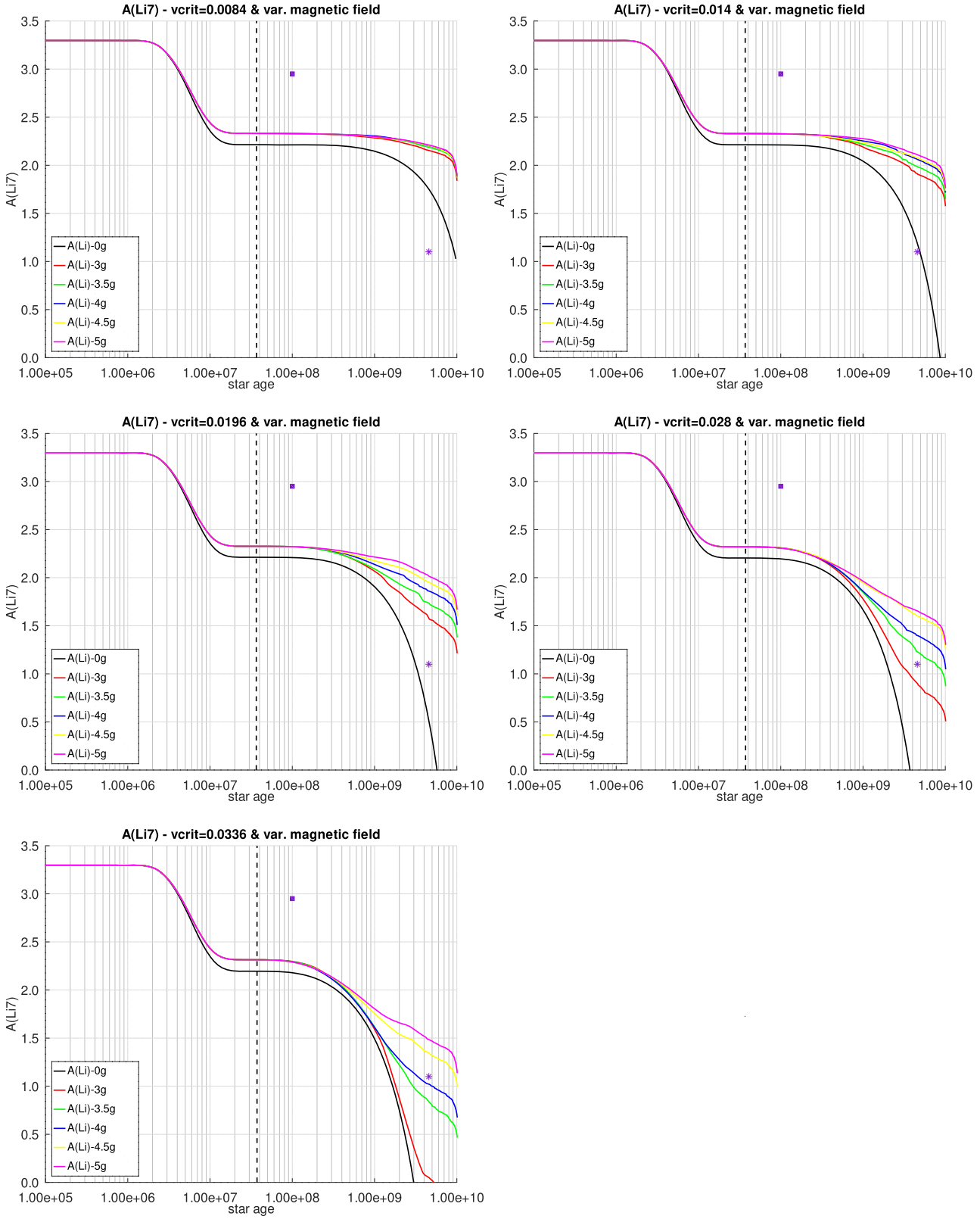

Figure A2. Grid showing the evolution of surface ^{7}Li abundance relative to ^{1}H, as a function of time for several 1 $M_{\odot}$ models. Each figure shows a set of models in which Ω/Ω_{crit} has been fixed and the magnetic field with intensity varies between 0.0 and 5.0 G, respectively. The purple star and square are surface Li abundance for the present-day Sun (Asplund et al. 2009) and the Pleiades cluster (Sestito & Randich 2005) respectively. The dashed vertical line makes reference to the ZAMS.

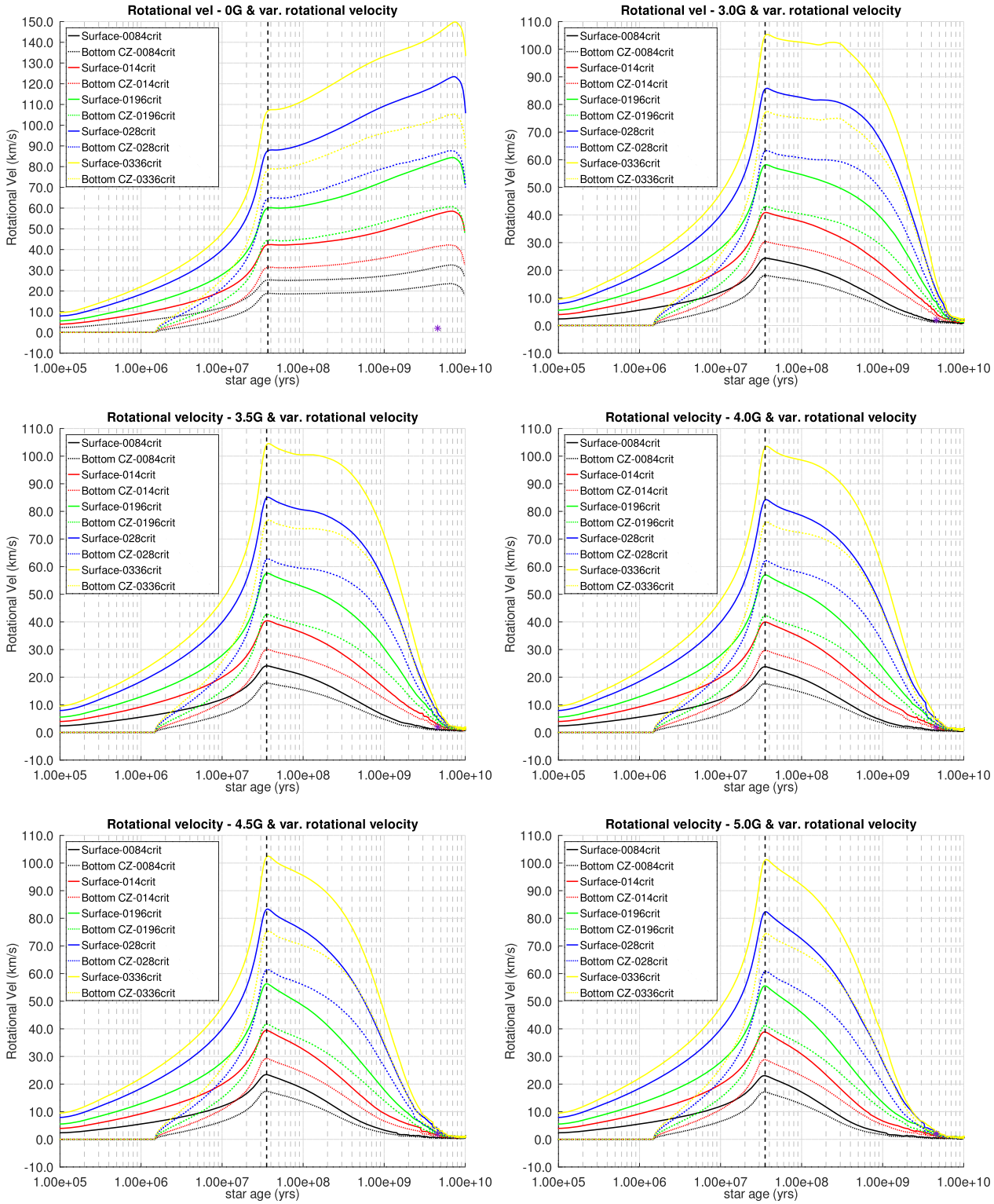

Figure A3. Grid showing of the evolution of surface rotational velocity, as a function of time for several 1 $M_{\odot}$ models. Each figure shows a set of models in which the magnetic field with intensity has been fixed and Ω/Ω_{crit} varies between 0.0084 and 0.0336. The purple star is the surface angular velocity for the present-day Sun (Gill 2012). The dashed vertical line makes reference to the ZAMS.

This paper has been typeset from a TEX/LATEX file prepared by the author.